

Fatigue-PINN: Physics-Informed Fatigue-Driven Motion Modulation and Synthesis

Iliana Loi, Konstantinos Moustakas

Abstract—Fatigue modeling is essential for motion synthesis tasks to model human motions under fatigued conditions and biomechanical engineering applications, such as investigating the variations in movement patterns and posture due to fatigue, defining injury risk mitigation and prevention strategies, formulating fatigue minimization schemes and creating improved ergonomic designs. Nevertheless, employing data-driven methods for synthesizing the impact of fatigue on motion, receives little to no attention in the literature. In this work, we present *Fatigue-PINN*, a deep learning framework based on Physics-Informed Neural Networks, for modeling fatigued human movements, while providing joint-specific fatigue configurations for adaptation and mitigation of motion artifacts on a joint level, resulting in more realistic animations. To account for muscle fatigue, we simulate the fatigue-induced fluctuations in the maximum exerted joint torques by leveraging a PINN adaptation of the Three-Compartment Controller model to exploit physics-domain knowledge for improving accuracy. This model also introduces parametric motion alignment with respect to joint-specific fatigue, hence avoiding sharp frame transitions. Our results indicate that *Fatigue-PINN* accurately simulates the effects of externally perceived fatigue on open-type human movements being consistent with findings from real-world experimental fatigue studies. Since fatigue is incorporated in torque space, *Fatigue-PINN* provides an end-to-end encoder-decoder-like architecture, to ensure transforming joint angles to joint torques and vice-versa, thus, being compatible with motion synthesis frameworks operating on joint angles.

Index Terms—Animation, PINNs, 3CC, Deep Learning, Biomechanics

I. INTRODUCTION

STUDING the effects of fatigue in human motion has been the focus of many biomechanical works [1]–[4], where the investigation of possible variations in movement patterns and posture and the inevitable decrease in maximum exerted torques and muscle forces as well as changes in the range of joint angles under fatigue conditions, is conducted. In contrast to typical biomechanics research, such as the previously mentioned studies that do not incorporate modeling of fatigued motions, data-driven approaches for estimating musculoskeletal dynamics (e.g. [5], [6]) offer promising and automated solutions for ergonomically-adjusted motion estimation. This includes fatigue-driven motion modeling, which is rather difficult to achieve without knowing the internal human state. Especially, joint torques are inextricably correlated with muscle activity and can be defined as a function of

joint angles [7]. Thus, the determination of joint torques is based on joint angles, velocities, and accelerations, i.e. Inverse Dynamics (ID), and vice versa, i.e. Forward Dynamics (FD). Machine and Deep learning approaches (ML/DL) for estimating physical movement parameters, such as joint contact forces (particularly those of the knee) [8], [9], joint torques [6], [10], and muscle forces [11], function as surrogate models for Inverse and Forward dynamics. These approaches can significantly enhance the simulation of physically-plausible 3D humanoid character movements. In recent years, state-of-the-art approaches such as Physics-Informed Neural Networks (PINNs), which embed physics-based domain knowledge into the training process, have been employed to bridge the gap between kinematics and dynamics estimation techniques [12]–[14].

However, fatigued-driven human motion generation using data-driven methods is yet to be explored despite its various advantages, like i) risk mitigation and prevention of injuries by understanding how fatigue affects movement patterns in both high-performance athletic [4] and non-athletic physically demanding occupations [15], ii) design of improved rehabilitation protocols by tailoring exercises that consider the impact of fatigue on muscle performance and joint stability [16], iii) optimized performance in athletes [17]–[19] and workers [20] by using strategies that minimize the negative effects of physical fatigue, iv) creation of better ergonomic designs (e.g. equipment, tools, workspaces, etc.) to reduce fatigue and enhance comfort and productivity [21], as well as v) the production of realistic simulations and physically-plausible fatigued-driven animation without the recording of strenuous motion capture (gaming) or handcrafted animation sequences (animation), which is essential for applications in virtual reality, gaming, ergonomic assessments, and rehabilitation.

To address this gap in literature, we introduce a deep learning framework based on PINNs, to produce fatigued open-type human movements. As open-type human motion we refer to both non-periodical movements and motions not involving human-object interactions. To account for muscle fatigue, we simulate the fatigue-induced fluctuations modulating joint torques of a 3D humanoid character. This simulation is grounded in a PINN adaptation of the Three-Compartment-Controller (3CC) Model [22]–[24], *3CC- λ* , a state machine that describes the transition of all muscle motor units of a human limb from one state (compartment) to another, namely active (M_A), fatigued (M_F), or resting (M_R) states. Given that the majority of motion synthesis frameworks produce sequences of joint angles, we devised an end-to-end encoder-decoder-like architecture, namely *Fatigue-PINN*, to incorporate fatigue effects within the torque space. In this setup, a

Iliana Loi, and Konstantinos Moustakas are with the Department of Electrical and Computer Engineering, University of Patras, Patras, 26504 Greece. Corresponding author: I. Loi. E-mail: loi@ceid.upatras.gr

This work has been submitted to the IEEE for possible publication. Copyright may be transferred without notice, after which this version may no longer be accessible.

surrogate DL model for ID converts joint angles into joint torques, then, the 3CC- λ model introduces fatigue to generate fatigued torques, which are afterward processed by a surrogate DL model for FD to perform the reverse transformation. Our semi-dynamics approach is joint-specific, meaning that Fatigue-PINN, is applied for estimating fatigue in each joint, ensuring the generation of realistic fatigue-driven animation without explicitly modeling the complex underlying physics that governs the human body and without the acquisition of fatigued motion capture data for training our models. Our contributions are summarized as follows:

- Introduction of Fatigue-PINN, an end-to-end automated PINN-based framework to model fatigue in open human movements by exploiting internal human state domain knowledge, bypassing the necessity of acquiring fatigued motion capture data. Our model provides joint-specific fatigue configurations allowing adaptation and mitigation of motion artifacts in a semi-automated manner, resulting in more realistic animations.
- Using 3CC- λ , a PINN variation of 3CC, to model fatigue in an automated and physically-consistent manner. PINNs exploit physics-based domain knowledge to constraint the estimation of the output, hence accelerating convergence and accuracy in cases of few training data.
- Provide robust deep learning methods to pose as semi-dynamics surrogate models for ID and FD procedures without taking into account Ground Reaction Forces (GRFs).
- The end-to-end encoder-decoder-like architecture of Fatigue-PINN, enables its seamless integration into any animation pipeline that operates on joint angles.

II. RELATED WORK

A. Data-Driven Motion Synthesis

In the motion synthesis area, researchers and developers in the graphics, animation, and gaming industries, dive deeply into both deterministic and probabilistic Deep Learning (DL) motion generation techniques. These data-driven approaches leverage human motion capture and movement history data (e.g., previous frames or motion states like joint angles) to produce or predict the pose and/or joint trajectories of a 3D humanoid character [25]. Especially for deterministic motion synthesis, where the synthesized motion sequence converges to a deterministic pose sequence that regresses towards the mean pose of ground-truth, recurrent architectures like LSTM models [26] for typical motion imitation and RNNs enhanced with phase-functioned networks [27]–[29] for scene-aware interactions, are favored. The work in [27], introduces the Neural State Machine (NSM), a framework for goal-driven real-time synthesis of 3D character movements and scene interactions. The NSM consists of a gating network and an RNN motion prediction network, where the first accounts for automatic action state transition based on the global phase of the motion signal and the user input (i.e. desired goal). In the subsequent works of the same authors [28], [29], an architecture similar to NSM is employed and enhanced with: i) a local phase feature that exploits the local motion

phases of each skeletal segment to dynamically produce their asynchronous motion in character-character, character-object, and character-scene interactions in [28], and ii) a control scheme in [29] for animation layering to produce sophisticated (e.g. martial arts movements) and novel motions based on reference motions, physics-based simulations, input controls, etc. Convolutional Neural Networks (CNNs) have also been employed for synthesizing human motion sequences [30].

On the contrary, Generative Adversarial Networks (GANs) [31], [32], Variational Autoencoders [33], [34], Transformers [35], [36], and the state-of-the-art diffusion models for motion generation conditioned on multiple sources (e.g. natural language descriptions and audio) [37]–[40], are exploited for probabilistic motion synthesis meaning the construction of all plausible pose sequences of a virtual character based on historical poses and/or control inputs. Probabilistic DL models have the ability to inject stochasticity in the training process, i.e. by fitting a latent distribution to the distribution of the next pose in each invocation, and, hence, increasing the learning capacity of the model.

Motion synthesis works can be used alongside musculoskeletal dynamics estimation approaches (described in Section II-B) to reflect the human internal state on a 3D humanoid character, thus, providing physics-based solutions. Consequently, works in the physics-based motion synthesis area develop holistic approaches, usually relying on Reinforcement Learning (RL) [41], [42], which account for the data-driven imitation of physically realistic motion sequences conditioned on physical parameters such as joint velocities, forces, torques, etc. It is worth mentioning the most recent work in [43], where an auto-regressive neural network resembling previous work [27]–[29], which incorporates knowledge from the physical attributes of exerted human force and perceived resistance, was applied to model variations in human movements while interacting with objects and, thus, enhancing realism.

Nevertheless, even though great steps are made towards more realistic computer graphics character animation, all the aforementioned methods and the ones referenced in Section II-B, focus on modeling the active state of human motion. Fatigued motion using DL has received little to no attention in the literature. To the best of our knowledge, only one work, the one in [44], attempts fatigue-driven animation, using RL methods for controlled motion imitation, and the Three-Compartment Controller (3CC) state machine to model torque-based fatigue.

B. Data-Driven Musculoskeletal Dynamics and Kinematics Estimation

Estimating musculoskeletal human biomechanics has been the focus of research for many years, with results affecting multiple research fields such as biomechanics, the gaming industry, robotics, and the animation industry. Biomechanics engineers use powerful open-source tools like OpenSim [45], to simulate with great precision human kinematics and compute the kinetics and dynamics of a motion (e.g. joint contact forces, joint torques, muscle forces, etc.), while state-of-the-art methods focus in data-driven approaches (ML/DL), such as

the ones in [5], [6], [8], [10] to obtain more automated, faster as well as real-time, solutions while estimating biomechanical variables traditionally calculated through musculoskeletal modeling. Such works rely on raw motion marker data, joint kinematics data (i.e. joint angles), Electromyography (EMG) data, and Ground Reaction Forces (GRFs) to infer predictions.

In [5] different feed-forward neural network configurations obtained through hyperparameter space exploration were trained and applied to estimate both joint biomechanical parameters (angles, reactions forces, torques) as well as muscle forces and activations in upper extremities. The authors concluded that more complex neural architectures with optimal parameters obtained through hyperparameter space search, lead to more accurate estimations. Furthermore, RNN models pose as the most common approaches in human biomechanics estimation [6], [8], [10]. In particular, in [8], a Bidirectional Long Short-Term Memory network (BiLSTM), augmented with unsupervised domain adaptation layers, was proposed to perform domain alignment between experimental data from various movements, with the goal to simultaneously generalize across multiple actions and align real-to-synthetic data. LSTM has also been utilized for ankle, knee, and hip joint torque estimation in sit-to-stand trials, alongside other machine learning (ML) and deep learning (DL) techniques such as Linear Regression (LR), Support Vector Machines (SVM), and Convolutional Neural Networks (CNN), as documented in [6], with LSTM indicating the best performance for the task. Similarly, LSTM and Gaussian Process Regression (GPR) were employed in [10] to predict lower extremity joint torques during gait.

C. Physics-Informed Neural Networks

Physics Informed Neural Networks, first introduced in [46], [47], are standard machine/deep learning models that incorporate the underlying physical laws of their training dataset, expressed as partial differential equations (PDEs), in the learning process (i.e. loss function) to address both forward and inverse problems. Forward problems involve approximating the PDEs governing the training dataset to derive solutions, without prior knowledge of the ground-truth, relying solely on the provided input data and respective boundary conditions. State-of-the-art works in fluid [48], [49] and quantum mechanics/computing [50], [51] utilize PINNs to solve forward problems, without explicitly modeling the underlying physics, unlike finite element and conventional physics-based methods. In inverse problems, PINNs leverage physics-based domain knowledge to penalize the estimation of physical quantities (i.e. limiting the solution space), enhancing robustness and generalization in cases of limited data availability as ground truth, where conventional ML/DL methods are rendered ineffective.

PINNs, despite being the revolution in the area of fluid and quantum mechanics, are also starting to be applied for biomechanics estimation tasks [12]–[14], [52]–[56]. In [12], [54], PINNs with CNNs as a base are used to predict muscle forces and joint angles based on EMGs, with the work in [54] developing a physics-based domain knowledge transfer technique to develop subject-specific PINN approaches.

Furthermore, in [56] a distributed physics-informed DL approach that builds local models acting on subdomains of EMG input data to enhance the efficiency and robustness of muscle forces and joint angle estimation, is presented, while in [53] a PINN-based approach for upper limb joint angle estimation under various loads is explored. In the most recent works [52], [55], involving the estimation of muscle parameters and joint angles [52] as well as joint torques [55] of the upper limbs, novel PINN architectures that incorporate Gated Recurrent Units (GRUs), are implemented. GRUs are a variant of RNNs with fewer training parameters and enhanced computational efficiency compared to LSTM models [57], [58], which significantly improve the accuracy of predictions involving time-dependent inputs and also support the learning of long-term time-dependencies. It is also worth mentioning the study in [13], which predicts muscle forces and identifies muscle-tendon parameters from unlabeled EMGs using both explicit and implicit PINN losses (i.e. describing the implicit relationship between muscle forces predicted by a DL model and those calculated by an embedded musculoskeletal model).

III. METHODOLOGY

Fatigue-PINN is a PINN-based deep learning architecture to produce fatigued human motion. Our framework consists of three joint-specific modules: i) the ID module to account for the transition from the joint kinematics to the joint torque domain, ii) the Fatigue module, a PINN adaptation of the Three-Compartment-Controller, namely 3CC- λ , to simulate the effects of fatigue on the synthesized motion and iii) an FD module to transform the fatigued torques into fatigued joint angles, as depicted in Figure 1.

In detail, at each motion frame t , the ID module is fed with a vector of N joint angles \mathbf{q}_t^N , which in our case corresponds to 32 joint angles including both the joints of upper (shoulder, elbow, wrist) and lower limbs (hip, knee, ankle), pelvis and lumbar and produces a vector of N joint torques $\hat{\tau}_t^N$. These torques are subsequently processed through the 3CC- λ model (Fatigue module) to generate fatigued torques ($\hat{\tau}_t^N$), which are then given as input to the FD module to yield the fatigued motion (i.e. fatigued joint angles $\hat{\mathbf{q}}_t^N$).

Even though our ID/FD BiLSTM model accurately estimates multiple joint torques and angles simultaneously (e.g., achieving approximately 86% testing accuracy for upper body joint torques and angles as shown in Table II), we opted for a joint-specific approach (as illustrated in Figure 1). This approach allows the neural network to focus all its learning capacity on a single task, resulting in enhanced accuracy, faster convergence, reduced training times, and lower computational requirements due to its reduced complexity. More specifically, the ID/FD model extracts latent space correlations from all joint angles (torques) to effectively produce predictions solely for one joint. This method allows for handling motion artifacts on a joint level while enabling the setting of joint fatigue profiles as discussed in Section III-B.

A. Dataset & Data Processing

To train our BiLSTM ID and FD models, we utilized the *Adapt Emotional Actions* open dataset, from the SIG Center

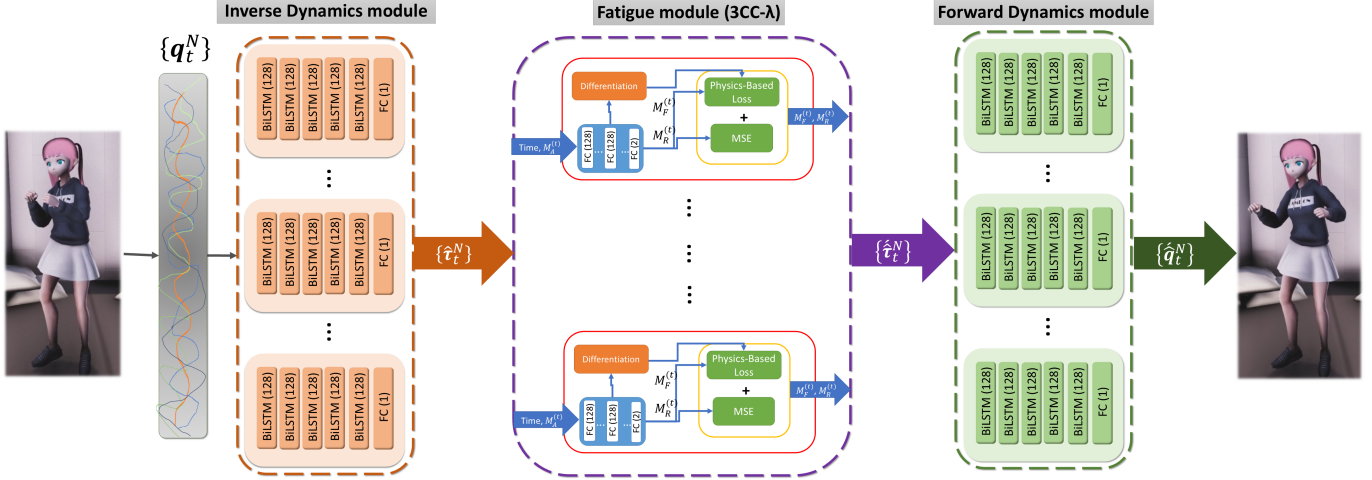


Fig. 1. General overview of our Fatigue-PINN framework.

for Computer Graphics Multi Modal Motion Capture Library of the University of Pennsylvania¹, that contains human motion capture data in C3D and BVH formats as well as force plate data (i.e. GRF data) from various activities, including knocking (a bell), box lifting, picking up pillow, pointing to spot, punching, box pushing, throwing, walking and waving. Each motion trial is expressed using a different emotion/behavior, based on the OCEAN model that provides a description of one’s personality over five dimensions: Openness (imagination and creativity), Conscientiousness (organization, carefulness), Extroversion (social aspect of human character), Agreeableness (friendliness, generosity, etc.), and Neuroticism (emotional instability, tendency towards negative emotions), with each factor being bipolar (+/–) and composed of several traits as cited in [59]. These personality traits, represented by the acronym OCEAN, are utilized to label each motion trial, meaning that the corresponding movement is performed to convey a specific emotion or behavior. For example, in the motion trial “Waving_E+_02”, the subject waves in a cheerful, energetic manner (i.e. E+ stands for Extroversion, thus, social, active, assertive, dominant, energetic behavior). Therefore, each movement consists of trials that are slightly different from one another, due to the expressed emotions, thereby introducing variability to the the dataset within each motion. This variability enhances the generalization capability of our BiLSTM models across different variations of the same movement.

Raw motion capture and GRF data are rotated to align with the OpenSim [45] coordinate system and converted into TRC and MOT formats (motion files’ formats) using Python scripts. These motion files are then utilized in the musculoskeletal modeling process in OpenSim to derive the ground-truth joint kinematics and corresponding joint torques for training our ID and FD models. The musculoskeletal model² utilized in OpenSim is the one introduced in [60], a Hill-type full-body model with muscle-actuated lower limbs (80 muscle-tendon

units) and torque-actuated torso/upper limbs (17 ideal torque actuators) with 37 Degrees of Freedom (DoFs) for describing joint kinematics.

The OpenSim analysis pipeline entails scaling the musculoskeletal model to match the anthropometric measurements of the subject used for capturing the Adapt Emotional Actions dataset. These measurements are obtained from the subject’s neutral pose marker data. Subsequently, the inverse kinematics (IK) procedure is employed to calculate joint angles for both the upper (i.e. arm flexion/adduction/rotation, elbow flexion/pronation and wrist flexion/deviation) and lower limbs (i.e. lumbar extension/bending/rotation, pelvis tilt/list/rotation, hip flexion/adduction/rotation, knee angle, ankle angle and subtalar angle) based on the spatial trajectories of the markers. Static Optimization is then performed to estimate muscle forces, which, along with the joint angles, are used to compute joint torques via ID. As for data pre-processing, the obtained joint kinematics and torques were normalized in the range $[0, 1]$ using the min-max normalization method.

B. 3CC

The Three-Compartment Controller, first introduced in [22], is a state machine that models the grouping of the muscle motor units of a human limb into three muscle activation states, as well as the transitions between them under static, [22] or dynamic load conditions [23], [24], [61], [62]. As depicted in Figure 2, at the beginning of a motion, motor units from the resting (M_R) state are transitioned to the active (M_A) compartment to satisfy the target load, TL (“required force” to fulfill a specific task). If more motor units are activated than the ones required to meet TL , some motor units may return to the resting state (from the M_A compartment to M_R). This bidirectional transfer of motor units between M_A and M_R is governed by a time-variant feedback controller, $C(t)$, which is dependent on TL as shown in Equation (4). During activity, motor units inevitably end up at the fatigued state compartment, M_F (i.e. their force start to decay over time), at a fatiguing rate, F , and, then, they enter rest period, i.e.

¹Available online at: <https://fling.seas.upenn.edu/~mocap/cgi-bin/Database>

²Available online at: https://simtk.org/projects/full_body/

moved to M_R , by a recovery rate of R . These transitions between the three states of 3CC in dynamic load conditions are described by the Equations (1), (2) and (3) [23], [24], [62]:

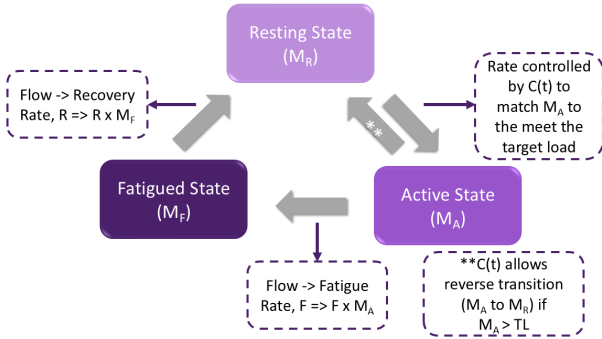


Fig. 2. 3CC. Figure reproduced from [24]

$$\frac{dM_R}{dt} = -C(t) + R * M_F \quad (1)$$

$$\frac{dM_A}{dt} = C(t) - F * M_A \quad (2)$$

$$\frac{dM_F}{dt} = F * M_A - R * M_F \quad (3)$$

$$C(t) = \begin{cases} L_D * (TL - M_A) & \text{if } M_A < TL \text{ and } M_R > (TL - M_A) \\ L_D * M_R & \text{if } M_A < TL \text{ and } M_R \leq (TL - M_A) \\ L_R * (TL - M_A) & \text{if } M_A \geq TL \end{cases} \quad (4)$$

The values of F and R are specific for every joint, as can be found in the literature [24] and depend on the task the muscles perform. A greater ratio between parameters F and R accounts for faster accumulation of fatigue as reported in [23], [24], [62]. Moreover, the parameters L_D and L_R , which contribute to the formulation of $C(t)$ in Equation (4), are constants that define respectively the ratio of muscle force development (L_D), thereby constraining the rate of muscle activation and the rate of muscle relaxation (L_R), ensuring the system's stability is preserved [23], [62].

Each one of the three compartments, M_A , M_F , and M_R are expressed in %MVC – maximum voluntary contractions, and by summing the percentage of muscle motor units in each compartment a total of 100% is obtained. Residual Capacity (RC) quantifies the remaining muscle strength or maximum exerted force/joint torque capability as a percentage, accounting for the effects of fatigue, and, thus, is defined as follows [23]:

$$M_A + M_F + M_R = 100\% \quad (5)$$

$$RC(t) = 100\% - M_F = M_A + M_R \quad (6)$$

Fatigue-PINN leverages a PINN version of 3CC, namely 3CC- λ , for modeling the fatigue state of specific muscle groups/joint actuator torques (w.r.t. the animated motion)

during open human movements. As shown in Figure 1, our PINN 3CC- λ is given as input the current active motor units M_A , which in our case are the joint torques of each DoF, $\hat{\tau}_t^N$, produced by the ID model, and outputs the percentage of motor units in the complementary states, M_F and M_R in MVC%. In contrast to previous work [44], we compute the RC of each joint, based on the M_F state multiplied by a λ factor (Equation (7)) that empirically describes the fatigue profile of each muscle/joint to better align joint fatigue in different movements and allow for joint-specific fatigue configurations. Subsequently, we apply RC as a time-varying factor to simulate the gradual decaying of the maximum exerted joint torques to directly generate the fatigued ones, $\hat{\tau}_t^N$, as in [23], [44] (Equation (8)):

$$RC(t) = 100\% - \lambda * M_F \quad (7)$$

$$\hat{\tau}_t^N = RC * \hat{\tau}_t^N \quad (8)$$

For instance, if $M_F = 20\%$, at elbow joint at frame t , and $\lambda = 0.6$ then from Equation (7) we derive that the maximum exerted elbow torques peak at $RC(t) = 88\%$ (instead of $RC(t) = 80\%$), meaning that λ factor, contributes in smoothly injecting joint-specific fatigue and producing more physically-plausible motions without intermittent ("step-like") movements.

As depicted in Figure 1, the 3CC- λ model consists of five fully connected layers, being fed with the current time frame t and current torque of each DoF, $\hat{\tau}_t^N$ (i.e. M_A), and produces M_F and M_R of the same frame. Its loss, L as formulated in Equations (9), (10), and (11), is comprised of two terms (in accordance with Figure 1) i) the Mean Squared Error (MSE) loss of the neural network, L_{NN} , and ii) the physics-based loss, L_{PB} , based on Equations (3) and (1) that describe the transition between the active and fatigued state and the transition between the fatigued and the resting state, respectively:

$$L = L_{NN} + L_{PB} \quad (9)$$

$$L_{NN} = \frac{1}{T} \sum_{t=0}^T (M_F - \hat{M}_F)^2 + \frac{1}{T} \sum_{t=0}^T (M_R - \hat{M}_R)^2 \quad (10)$$

$$L_{PB} = \frac{1}{T} \sum_{t=0}^T \left(\frac{d\hat{M}_F}{dt} - F * M_A + R * \hat{M}_F \right)^2 + \frac{1}{T} \sum_{t=0}^T \left(\frac{d\hat{M}_R}{dt} + C(t) - R * \hat{M}_F \right)^2 \quad (11)$$

where \hat{M}_F and \hat{M}_R represent the percentage of motor units at the fatigued and resting states as estimated by the neural network and M_F and M_R correspond to the ground-truth values.

To simulate the flow between the compartments of 3CC, we train our PINN using datasets referenced in [62], such as the one in [63]. Such datasets, explore the fluctuations of joint actuator torques after a fatiguing task based on experimental setups (e.g. measuring joint torques after a series of MVCs

of a corresponding muscle set). Given the very few data in these datasets (i.e. $\sim 40 - 50$ time frames), the physics-based loss penalizes the neural network's predictions, thus, limiting the solution space and better guiding the learning process. In simpler words, these datasets aid the PINN model to learn the functionality of the 3CC faster, leading to accelerated convergence (typically within ~ 50 epochs). As mentioned in Section V-A, the 3CC- λ network can be also trained unsupervisingly, where only the loss term L_{PB} contributes to the training procedure.

Furthermore, F and R , are set to values specific for every joint upon which the 3CC- λ is applied. For example, for the elbow joint, the parameters are set to $F = 0.00912$ and $R = 0.00094$ values, according to [24]. Constants L_D (rate of muscle force development) and L_R (rate of muscle relaxation) are set to 10 for all joint configurations [23]. It is worth mentioning that L_D and L_R have the least influence on the predicted fatigue since the temporal progression of muscle force development and relaxation factor is negligible to the one of fatigue as explained in [23]. The training of 3CC- λ was conducted using Python's Keras library [64] employing the adaptive moment estimation (Adam) [65] optimizer with a batch size of 32 and a learning rate of 0.001, to improve the training convergence and prevent gradient descent from getting stuck at local minima.

C. Inverse/Forward Dynamics Model

In both motion synthesis and musculoskeletal dynamics estimation research, RNNs are preferred over other machine learning methods. This preference arises from their ability to extract temporal features from motion sequences, which is essential for motion and dynamics estimation (within the same time frame t), prediction (for the subsequent time frame $t+1$), and the synthesis of novel movements.

In this work, we exploit Bidirectional Long Short-Term Memory neural networks to develop both our ID and FD surrogate models, which produce precise predictions without requiring GRFs for their training. BiLSTMs possess two parallel sequences of forward and backward feedback connections, in contrast to LSTMs, which have only a single forward loop. This dual-sequence architecture enables BiLSTMs to handle both past and future time dependencies effectively, preventing gradients from gradually vanishing during training and thereby producing more accurate predictions [66], [67].

The forward and backward sequence outputs are computed using Equations (12) and (13), which are the standard LSTM updating equations [66]–[68]. In particular, the output \vec{h}_t of the forward sequence is computed iteratively in a positive time direction spanning from $t = T$ to time $t = 1$. On the contrary, the backward loop is "looking" at the past, thus, its output \overleftarrow{h}_t is calculated in a negative time direction from $t = 1$ to $t = T$ (see Figure 3):

$$\vec{h}_t = g(U_{\vec{h}} x_t + W_{\vec{h}} \vec{h}_{t-1} + b_{\vec{h}}) \quad (12)$$

$$\overleftarrow{h}_t = g(U_{\overleftarrow{h}} x_t + W_{\overleftarrow{h}} \overleftarrow{h}_{t-1} + b_{\overleftarrow{h}}) \quad (13)$$

where x_t , is the input data x at time frame t , U and W are the weight matrices and b is the bias vector. The input of the ID model, is defined as $x_t = \mathbf{q}_t^N$, i.e. a vector of N joint angles at frame t , while $x_t = \hat{\tau}_t^N$ is the input for the FD model, i.e. a vector of N fatigued torques at time t . The values of the weight matrices and the bias vector are updated ("learned") during training.

Furthermore, the BiLSTM layer produces an output vector at each time frame t , y_t , which is computed using the calculated feedback sequences' outputs, \vec{h}_t and \overleftarrow{h}_t , as indicated by Equation (14) [67].

$$y_t = g(V_{\vec{h}} \vec{h}_t + V_{\overleftarrow{h}} \overleftarrow{h}_t + b_y) \quad (14)$$

where in our case g is a concatenating function used to combine the outputs of the two feedback sequences [68]. Given that y_t , is the output of the last BiLSTM layer in each of ID/FD architecture, it is then passed to a fully connected layer (as illustrated in Figures 1 and 3). In our joint-specific framework, the fully connected layer in the ID model computes the current torque for one joint denoted as $\hat{\tau}_t$, while the fully connected layer of the FD architecture produces a single fatigued joint angle, \hat{q}_t , at frame t .

As shown in Figures 1 and 3, the ID and FD models utilize a symmetric BiLSTM architecture consisting of five BiLSTM layers each one of them containing 128 units with linear activation on the first BiLSTM layer and ReLU activations on the rest hidden layers. Additionally, a Fully Connected layer with linear activation is included as the output of the ID/FD models. Similarly to the training of 3CC- λ , both ID and FD BiLSTM networks were trained in Python Keras, utilizing the Adam optimizer with a learning rate of 0.001. The learning process was conducted with a batch size of 32 and a MSE loss function, over 1000 epochs, with early stopping enabled to prevent the model from over-fitting.

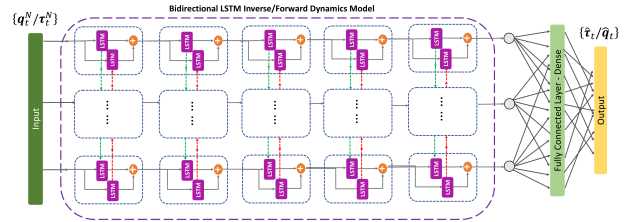


Fig. 3. BiLSTM Inverse/Forward Dynamics Model. The feedback loop of each BiLSTM layer is marked with green arrows, whereas its backward sequence is indicated with red arrows.

IV. RESULTS

A. Fatigue Effects in Animation

The proposed Fatigue-PINN framework was trained and tested upon open-type movements (as defined in this work), i.e. waving, punching, throwing, to assess its capability of effectively producing fatigued motion in various action classes (see Figure 4). We opted to apply fatigued torques on the upper body (shoulders, elbows, wrists, and lumbar), whose motion is



Fig. 4. The impact of different levels of fatigue on punching (Frame 290, i.e. the moment of hit), throwing (Frame 240, at throw), and waving (Frame 100) motions. The levels of fatigue are defined w.r.t Residual Capacity as arises from Equation (8). For instance, 30% fatigue $\rightarrow RC(t) = 70\%$, etc.

crucial for perceiving the effects of fatigue in these particular open motions. Our results are simulated in Unity Game Engine Environment [69], utilizing the *Anime Girl Character*³ avatar from Unity Asset Store.

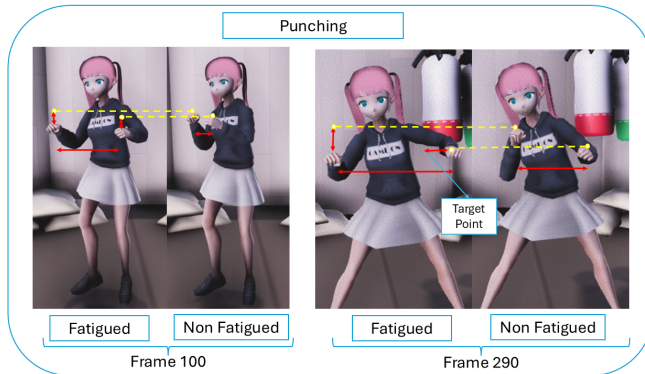


Fig. 5. Effects of fatigue on punching motion. At frame 100 the character is at guard stance, and frame 290 exhibits the moment of impact of the left hand. The discrepancies in hand positioning are marked with yellow dotted lines, while the distances between fatigued and non-fatigued hand positions are marked with red arrows.

In both motion frames depicted in Figure 5, the character on the left exhibits fatigued movement ($RC(t) \approx 55\%$) in all joints of both arms, while the right is the non-fatigued one. In punching motion (Figure 5), the hand positioning is different than in the non-fatigued motion, rendering the fatigued character "unguarded" to hits (see frame 100 in Figure 5). Moreover, in frame 290 as shown in the right section of Figure 5, another discrepancy in motion due to fatigue is apparent,

with both arms performing a wider movement while hitting, thus, missing the target. These two effects on the kinesiology of the 3D character, guard drop, and non-accurate punches, are behaviors observed alongside the increase of perceived fatigue in boxing athletes [18], [19], while guard drops pose as a tactical strategy to mitigate fatigue by providing a small period of rest [18]. The latter, known as a pacing strategy, involves the adaptation of exercise intensity (decrease/increase effort accordingly) to minimize the impact of fatigue and thereby attain the desired outcome [17] (e.g. determine the winner in a boxing bout). Moreover, the "unguarded" stance is a result of increased shoulder abduction, therefore, decreased shoulder adduction as seen in Section A of Figure 9, and increased elbow extension (i.e. less flexed elbow as in Figure 9). Notably, while shoulder adduction generally decreases, it increases at the moment of hitting impact (around frame 250), resulting in a corresponding decrease in shoulder abduction. These findings align with those in [3]. Lumbar flexion and rotation are reduced, with the character inclining to the left during striking, while the upper body exhibits greater rotation to the right. These discrepancies in joint angles are reflected in the respective torques, which are expected to be reduced in presence of fatigue by the 3CC- λ model.

Similar results are observed in throwing (see Figure 6), with the right hand, the one performing the motion, being directed in a lower position than the one intended. The externally perceived impact of fatigue in this movement can be associated with the one in pointing tasks [2], [70], where one hand extends towards a specific position while the other remains relatively inactive. However, throwing is inherently more physically demanding, thereby we intuitively expect it to lead to a more pronounced fatigue effect. Regarding the

³Available online at: <https://assetstore.unity.com/packages/3d/characters/humanoids/casual-1-anime-girl-characters-185076#publisher>

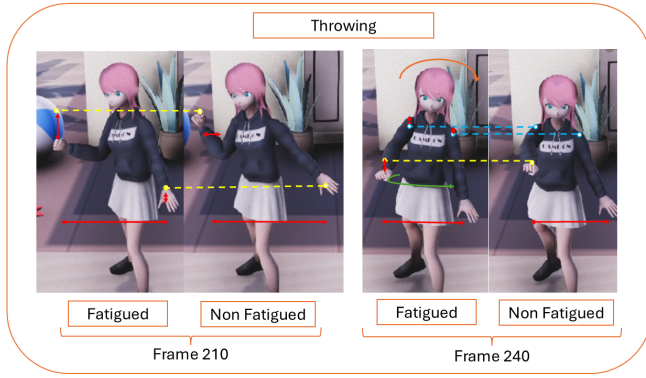


Fig. 6. Effects of fatigue on throwing motion. Frame 210 indicates the pre-throwing phase, and frame 240 depicts the moment of throwing. The changes in hand positioning between fatigued and non-fatigued motion are marked with yellow dotted lines, while the discrepancies in shoulder positions are marked in cyan dotted lines. Moreover, the increased flexion towards the left side (i.e. decreased lumbar bending angle in the lateral plane) is noted with an orange arrow, whereas a green arrow illustrates lumbar left rotation.

changes in position as depicted in the right section of Figure 6 (frame 240), the shoulder joint positions of both arms are moving towards the non-throwing side, while the right shoulder is positioned higher at throw, which is in accordance with the findings in [70], and may provide compensation mechanisms for the increased shoulder elevation and elbow extension [70], [71]. Moreover, following fatigue, the shoulder and elbow joints of the right arm (the one performing the throwing/pointing task) adopt a more posterior position, indicating a posture that reduces shoulder torques [70] (Figure 7), consistent with the predictions of the 3CC- λ model.

Similar to the findings in [2], [70], the fatigued character in the left of Figure 7, exhibits reduced shoulder flexion of the right hand at the moment of throwing (frame 240). Akin to the results in [70], upper-body inclination towards the non-reaching arm’s side due to decreased lumbar bending angle (i.e. more flexion in the lateral plane towards the left side) is also evident at throw (Frame 240 in Figure 6). Moreover, in accordance to [2], greater lumbar rotation (i.e. increased lumbar left rotation angle) throughout throwing (frames 210 – 300) is apparent in fatigued movement as illustrated in Figures 6 and 9 (Section B). The above kinematic effects are attributed to elbow and/or shoulder fatigue, as observed in [1], [2], [70].

Furthermore, the right-hand elbow is less flexed (reduced elbow flexion angle as seen in Figures 6 and 9), which is considered a mean of compensation for both elbow and trunk fatigue as mentioned in [2], whereas elbow fatigue also influences shoulder abduction/adduction, leading to increased abduction (i.e. decreased adduction as shown in Figure 9) [2].

The effects of fatigue are also evident in waving movement, where the elbow of the right (i.e. waving hand) is rendered more extended, resulting in a limited range of motion (Section C in Figure 9 and Figure 8). Overall, the greater the decrease in percent of maximum exerted torques (i.e. greater $RC(t)$ as arises from Equation (8)) the more the influence of fatigue in the produced motions.⁴

⁴Please refer to the videos in the supplemental material for more qualitative results regarding our framework.

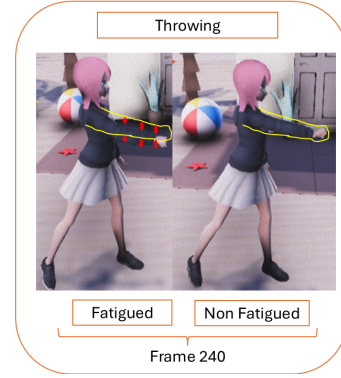


Fig. 7. Profile shots of throwing motion at frame 240 (moment of throwing). At throw, the right shoulder and elbow are positioned more posterior, while the arm is positioned lower due to decreased shoulder flexion.

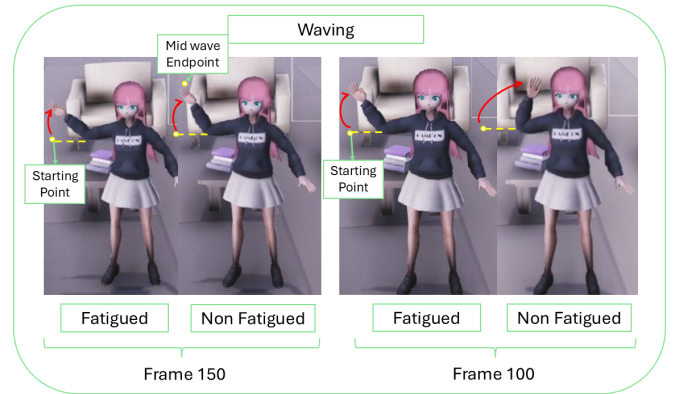


Fig. 8. Effects of fatigue at waving motion. The starting and midwave points of the movement are indicated by yellow markers, while the angle between the waving right hand and the starting point is denoted by red arrows.

B. Accuracy Results

In Table I we provide the Normalised Root Mean Squared Error (NRMSE) values for joint-specific ID and FD models of Fatigue-PINN framework across different actions. NRMSE values indicate the discrepancies between ground truth and predicted joint angles/torques during the testing of the models, thus, smaller values signify good accuracy. As observed in Table I all values are < 1 , consequently, our models perform quite well in new (unseen) data.

To further support the selection of a joint-specific approach, i.e. apply Fatigue-PINN for each joint angle, against the non-joint-specific, we provide the Pearson’s Correlation Coefficient, R^2 , values to evaluate the precision of the two methods. R^2 evaluates the correlation between the predicted joint torques/angles and their real values, with values closer to 1 indicating better alignment. As shown from Table II the predictions of the ID and FD models of the joint-specific architecture tend to be more correlated (higher R^2) with the ground-truth values, than the ones of the non-joint-specific approach, providing an insight of average testing accuracy for the former method being $\sim 97\%$, in contrast of average testing precision for the non-joint-specific, $\sim 86\%$. As expected, the joint-specific Fatigue-PINN architecture enhances the preci-

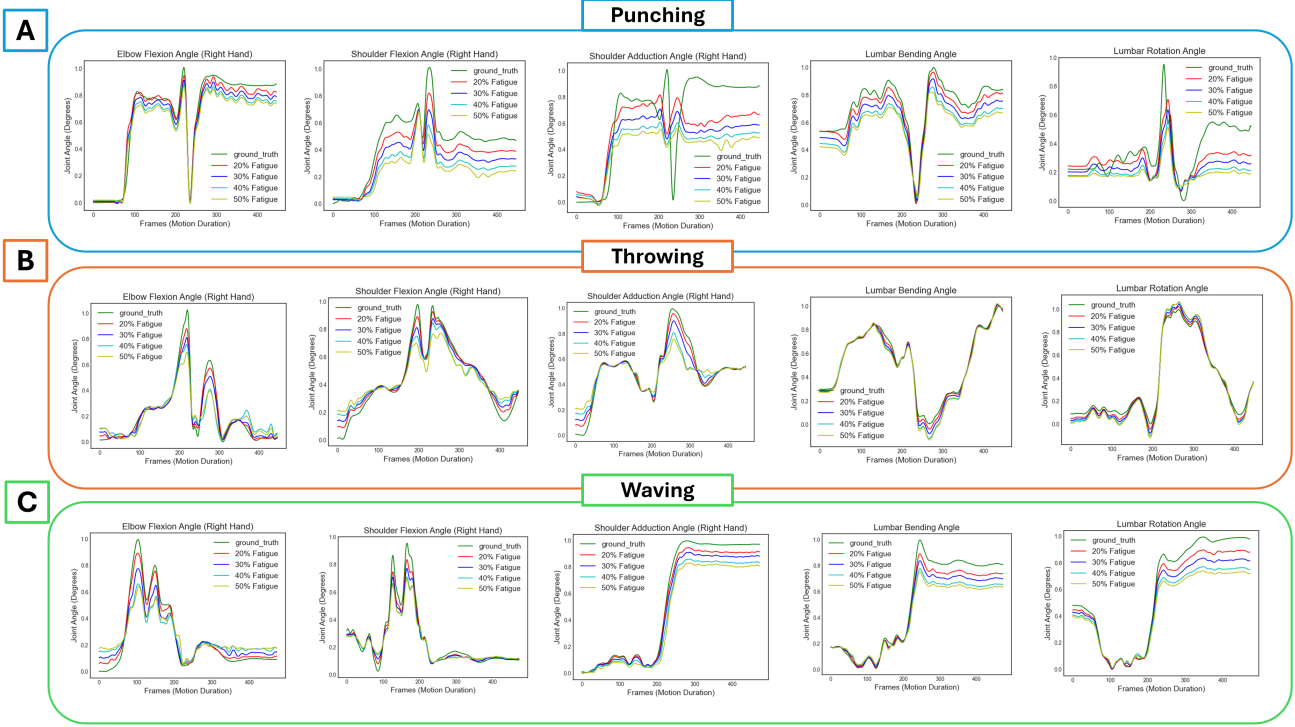


Fig. 9. The impact of fatigue on lumbar bending and rotation, as well as elbow flexion, shoulder flexion, and shoulder adduction angles of the right arm during the movements of punching, throwing, and waving (Sections A, B, and C, respectively). The effects of various levels of fatigue are demonstrated; for instance, 20% of fatigue corresponds to the exertion of 80% of maximum torque from the respective joints. The results are outlined in the range of $[0, 1]$.

TABLE I
NRMSE FOR ID/FD MODELS

NRMSE values For Right Upper Limb Joint Torques/Angles							
Motion	arm_flex	arm_add	arm_rot	elbow_flex	elbow_pro	wrist_flex	
Punching	0.17/0.72	0.11/0.90	0.91/0.36	0.75/0.13	0.16/0.37	0.27/0.99	
Throwing	0.49/0.58	0.12/0.57	0.28/0.69	0.39/0.62	0.14/0.56	0.19/0.74	
Waving	0.21/0.24	0.23/0.24	0.11/0.72	0.31/0.25	0.93/0.19	0.58/0.14	
NRMSE values For Right Lower Limb Joint Torques/Angles							
Motion	hip_flex	hip_add	hip_rot	knee_angle	ankle_angle	sub_angle	
Punching	0.19/0.20	0.23/0.79	0.37/0.55	0.17/0.28	0.45/0.71	0.57/0.63	
Throwing	0.10/0.57	0.20/0.62	0.39/0.65	0.73/0.50	0.80/0.79	0.13/0.67	
Waving	0.35/0.32	0.41/0.15	0.10/0.18	0.40/0.20	0.27/0.12	0.34/0.25	
NRMSE values For Joint Torques/Angles of the Torso							
Motion	pelv_tilt	pelv_list	pelv_rot	lumb_ext	lumb_bend	lumb_rot	
Punching	0.22/0.15	0.29/0.28	0.35/0.30	0.16/0.31	0.25/0.24	0.16/0.32	
Throwing	0.99/0.12	0.19/0.57	0.71/0.44	0.38/0.58	0.66/0.71	0.52/0.58	
Waving	0.37/0.20	0.36/0.30	0.19/0.15	0.20/0.29	0.30/0.39	0.59/0.64	

^a NRMSE values for joint torques/angles of the right upper and lower limb as well as torso, across punching, throwing, and waving motions. The first values in each row indicate the NRMSE values produced by the joint-specific ID models while the second values (after the "/") denote the NRMSE values for joint-specific FD models.

sion of animations by leveraging neural networks to extract latent space correlations from all joint torques/angles in order to efficiently accomplish a single task. It is worth noting that the R^2 values are computed for the joint torques/angles of the

upper right limb and during punching motion. Similar results with minimum differences $\sim 1 - 2\%$ are observed in the other two movements as well as the rest of the joints.

TABLE II
 R^2 FOR JOINT-SPECIFIC AND NON-SPECIFIC APPROACHES

R^2 values For Right Upper Limb Joint Torques/Angles during Punching							
Motion	arm_flex	arm_add	arm_rot	elbow_flex	elbow_pro	wrist_flex	
JS Model	0.97/0.96	0.90/0.91	0.96/0.95	0.94/0.96	0.93/0.97	0.94/0.95	
NJS Model	0.88/0.90	0.81/0.85	0.84/0.88	0.85/0.87	0.82/0.89	0.81/0.82	

^b Pearson's Correlation Coefficient values (R^2) for predictions of ID (estimating joint torques) and FD (estimating joint angles) models, during punching motion. A comparison of R^2 values between the Fatigue-PINN joint-specific approach and the non-joint-specific approach is provided. Thus, JS stands for "Joint-Specific", and NJS, for "Non-Joint-Specific" models. Just as in I, R^2 values of the ID models are presented first, while the second values (after the "/") denote the R^2 values for the respective FD models.

V. DISCUSSION

A. Ablations

Within Fatigue-PINN, we modeled our ID and FD networks as PINNs as well. The primary distinction in our corresponding BiLSTM networks lies in the loss function, where, in addition to the MSE term, which minimizes the loss between the neural network estimations and the real values of joint actuator torques (for ID) and joint angles (for FD), we incorporated a physics-based loss term derived from the classical equation of

motion (Equation (15)). This equation denotes the relationship of joint kinematics (generalized positions, i.e. joint angles, velocities, and accelerations), with generalized forces (i.e. joint torques) during human motion:

$$L_{PBID} = \frac{1}{N} \sum_{n=1}^N \sum_{t=0}^T (M(\mathbf{q}_t^n) \ddot{\mathbf{q}}_t^n + C(\mathbf{q}_t^n, \dot{\mathbf{q}}_t^n) + G(\mathbf{q}_t^n) - \tau_t^n)^2 \quad (15)$$

where, N is the number of DoFs, $M(\mathbf{q}_t^n) \in R^{N \times N}$ is the Mass matrix, $C \in R^N$ is the Coriolis and Centrifugal forces vector and $G \in R^N$ is the Gravitational forces vector, while $\mathbf{q}, \dot{\mathbf{q}}, \ddot{\mathbf{q}} \in R^N$ are the vectors of generalized positions, velocities, and accelerations respectively, and τ_t^n represent joint torques.

Nevertheless, the changes in model accuracy and generated fatigued motion are insignificant whether we use PINNs to formulate our ID and FD models or not (the NRMSE values of the ID/FD PINN models differ by about $\pm 5\%$ compared to those in Table I). Therefore, even though we utilized the standard BiLSTM architecture for the ID and FD models, their PINN versions offer a viable solution in cases of limited data availability. This is because PINN loss functions act as soft physical constraints during human motion, facilitating the inference of corresponding joint torques and angles.

It is worth mentioning that we also experimented with training the 3CC- λ unsupervisedly (solving the forward problem), where no ground-truth data for fatigued, M_F , and resting state M_R , are provided. In this case, the PINN loss, L (see Equation (9)), still has its physics-based term, L_{PB} (Equation (11)), and instead of L_{NN} (Equation (10)), we add a loss term to incorporate boundary conditions regarding M_F and M_R . However, training 3CC- λ unsupervisedly requires more computational resources compared to the approach outlined in Section III-B.

B. Fatigued Movements

Fatigue is usually neglected in most musculoskeletal models as well as in data-driven motion synthesis frameworks, leading in bypassing an element that could significantly boost animation realism. The widely emerging Physics-Informed Neural Networks are also making their debut in human biomechanics estimation tasks (e.g. prediction of joint angles/forces/moments, muscle forces, etc. [12]–[14], [52]–[56]) since they can inject physics-based domain knowledge into the learning procedure to both approximate PDEs describing the problem-to-solve (e.g. Inverse of Forward Kinematics equations) and penalize solutions not adhering to physical laws, limiting the solution space, which leads to faster convergence during training. Consequently, PINNs provide more accurate physically consistent solutions, while requiring a significantly smaller amount of data to approximate the underlying physical laws.

In this study, we present Fatigue-PINN, an advanced end-to-end PINN-based deep learning framework to synthesize fatigued human motion without relying on fatigued motion capture data for training. Our architecture is composed of three modules, the Inverse Dynamics Module, which translates

input joint angles into joint torques, the Fatigue module, i.e. the 3CC- λ model to simulate the effects of fatigue in the maximum exerted joint torques, and the Forward Dynamics model, which transforms these fatigued joint torques back into joint angles, thus enabling the fatigued animation of a 3D character. 3CC- λ is a PINN adaptation of the 3CC state machine [22]–[24], augmented with a method to account for joint-specific fatigue configurations, thereby ensuring seamless incorporation of fatigue effects in different motions and avoid sharp step-wise motions. Additionally, we use ID and FD models employed upon each DoF. These joint-specific models enhance predictive accuracy and are also compatible with the joint-specific fatigue profiles as defined by 3CC- λ . By having control at the joint level, our model is capable of generating physically plausible movements with reduced motion artifacts. The ID and FD models are LSTM-based to extract the temporally evolving fatigue impact and can be utilized as surrogate models to perform the respective tasks without the need of GRFs.

Our results indicate that Fatigue-PINN produces realistic fatigue effects on open-type movements, which are consistent with the existing literature [2], [3], [18], [19], [70]. It is worth mentioning that in our experiments, all upper body muscles were fatigued isometrically, causing overlapping kinematic changes to render the externally perceived fatigue impact more evident. Nevertheless, since our Fatigue-PINN framework is joint-specific it can also be utilized to study the effects of fatigue on posture and joint kinematics after inducing localized muscular fatigue (e.g. fatiguing shoulder and observing the impact on elbow and trunk), just as in [2], where no data-driven method was used.

Furthermore, our end-to-end Fatigue-PINN framework can be utilized to both facilitate the work of animators and aid biomedical engineers with investigating the effects of externally perceived fatigue on posture and movements. By simply providing a motion sequence (i.e. a sequence of joint angles), the fatigued movement at a specified level of fatigue, is synthesized. Fatigue-PINN does not require direct input of joint torques for fatigue incorporation, as it can convert joint angles into torques and vice versa. The latter enables the seamless integration into motion synthesis pipelines that operate on joint angles.

A limitation of our work is that even though it succeeds in modeling fatigue in closed-type movements, i.e. when an object is involved, such as lifting or pushing a box, it lacks in accuracy, with motion artifacts being present, mostly in the end effectors. A possible solution to fix hand artifacts is to incorporate in our framework contact points [27], [28] as well as forces produced by the human-object interactions. As for foot contact artifacts, exploiting GRFs and foot contact information [32] as well as utilizing GANs [72] or diffusion models [37], are possible ways to mitigate these artifacts. The latter is proposed as future work.

VI. CONCLUSION

Addressing the gap of data-driven methods for modeling fatigue in literature, we introduce Fatigue-PINN, a PINN-based deep learning framework for synthesizing fatigued hu-

man movements without explicitly modeling the complex underlying physics laws governing the human body. Our framework consists of three modules, namely Inverse Dynamics, Fatigue, and Forward Dynamics modules, forming an encoder-decoder-like architecture for producing fatigued joint angle sequences based on fatigued-induced joint torques. Despite the incorporation of fatigue within the torque space, the end-to-end encoder-decoder configuration processes joint angles to produce their fatigued adaptations, facilitating the integration with any motion synthesis model functioning on joint angles and testing the real-time capabilities of the system. To estimate the fatigued state of motion, we model the 3CC state machine as a PINN, 3CC- λ , and we enhance it with the parameter λ to characterize the fatigue profile of each joint and contribute to the smooth integration of fatigue in produced motion, thus, preventing abrupt frame transitions. Our semi-dynamics joint-specific approach, employing an ID and FD BiLSTM model for each joint, not only improves the overall predictive accuracy but also enables better alignment with joint-specific fatigue configurations and handling motion artifacts. Fatigue-PINN simulates the effects of externally perceived fatigue on open-type human movements comparable with findings from real-world experimental fatigue studies, even though it does not require fatigued motion capture data for the learning process. The adaptation of Fatigue-PINN to closed-type movements involving contacts and forces in human-object interactions remains as a future research direction.

ACKNOWLEDGMENTS

The data used in this project was obtained from <https://fling.seas.upenn.edu/~mocap/cgi-bin/Database>. The research project is implemented in the framework of H.F.R.I call “Basic research Financing (Horizontal support of all Sciences)” under the National Recovery and Resilience Plan “Greece 2.0” funded by the European Union – NextGenerationEU (H.F.R.I. Project Number: 16469.).

REFERENCES

- [1] J. Cowley and D. Gates, “Proximal and distal muscle fatigue differentially affect movement coordination,” *PLOS ONE*, vol. 12, no. 2, p. e0172835, 02 2017.
- [2] C. Yang, S. Leitkam, and J. N. Côté, “Effects of different fatigue locations on upper body kinematics and inter-joint coordination in a repetitive pointing task,” *PLoS One*, vol. 14, no. 12, 12 2019.
- [3] N. Haralabidis, D. J. Saxby, C. Pizzolato, L. Needham, D. Cazzola, and C. Minahan, “Fusing accelerometry with videography to monitor the effect of fatigue on punching performance in elite boxers,” *Sensors*, vol. 20, no. 20, p. 5749, 2020.
- [4] Z. He, G. Liu, B. Zhang, B. Ye, and H. Zhu, “Impact of specialized fatigue and backhand smash on the ankle biomechanics of female badminton players,” *Scientific Reports*, vol. 14, p. 10282, 05 2024.
- [5] R. Sharma, A. Dasgupta, R. Cheng, C. Mishra, and V. H. Nagaraja, “Machine learning for musculoskeletal modeling of upper extremity,” *IEEE Sensors Journal*, vol. 22, no. 19, pp. 18 684–18 697, 2022.
- [6] M. Mansour, K. Serbest, M. Kutlu, and M. çilli, “Estimation of lower limb joint moments based on the inverse dynamics approach: a comparison of machine learning algorithms for rapid estimation,” *Medical & biological engineering & computing*, vol. 61, no. 8, 08 2023.
- [7] D. Anderson, M. Madigan, and M. Nussbaum, “Maximum voluntary joint torque as a function of joint angle and angular velocity: Model development and application to the lower limb,” *Journal of biomechanics*, vol. 40, no. 14, pp. 3105–13, 02 2007.
- [8] I. Loi, E. I. Zacharaki, and K. Moustakas, “Multi-action knee contact force prediction by domain adaptation,” *IEEE Transactions on Neural Systems and Rehabilitation Engineering*, vol. 32, pp. 122–132, 2024.
- [9] J. Zou, X. Zhang, Y. Zhang, and Z. Jin, “Prediction of medial knee contact force using multisource fusion recurrent neural network and transfer learning,” *Medical & Biological Engineering & Computing*, vol. 62, no. 6, 01 2024.
- [10] M. Wang, Z. Chen, H. Zhan, J. Zhang, X. Wu, D. Jiang, and Q. Guo, “Lower limb joint torque prediction using long short-term memory network and gaussian process regression,” *Sensors*, vol. 23, no. 23, 2023.
- [11] A. Sohane and R. Agarwal, “Knee muscle force estimating model using machine learning approach,” *The Computer Journal*, vol. 65, no. 5, pp. 1167–1177, 2022.
- [12] J. Zhang, Y. Zhao, F. Shone, Z. Li, A. F. Frangi, S. Q. Xie, and Z.-Q. Zhang, “Physics-informed deep learning for musculoskeletal modeling: Predicting muscle forces and joint kinematics from surface emg,” *IEEE Transactions on Neural Systems and Rehabilitation Engineering*, vol. 31, pp. 484–493, 2023.
- [13] S. Ma, J. Zhang, C. Shi, P. Di, I. D. Robertson, and Z.-Q. Zhang, “Physics-informed deep learning for muscle force prediction with unlabeled semg signals,” *IEEE Transactions on Neural Systems and Rehabilitation Engineering*, vol. 32, pp. 1246–1256, 2024.
- [14] Z. Zhang, Y. Zhu, R. Rai, and D. Doermann, “Pimnet: Physics-infused neural network for human motion prediction,” *IEEE Robotics and Automation Letters*, vol. 7, no. 4, pp. 8949–8955, 2022.
- [15] D. Jo and H. Kim, “The influence of fatigue, recovery, and environmental factors on the body stability of construction workers,” *Sensors*, vol. 24, no. 11, 2024.
- [16] M. Carratalá-Tejada, A. Cuesta-Gómez, R. Ortiz-Gutiérrez, F. Molina-Rueda, L. Luna-Oliva, and J. C. Miangolarra-Page, “Reflex locomotion therapy for balance, gait, and fatigue rehabilitation in subjects with multiple sclerosis,” *Journal of Clinical Medicine*, vol. 11, no. 3, 2022.
- [17] B. L. Smits, G.-J. Pepping, and F. J. Hettinga, “Pacing and decision making in sport and exercise: the roles of perception and action in the regulation of exercise intensity,” *Sports Medicine*, vol. 44, no. 6, pp. 763–775, 2014.
- [18] E. C. Dunn, C. E. Humberstone, K. F. Iredale, D. T. Martin, and A. J. Blazevich, “Human behaviours associated with dominance in elite amateur boxing bouts: A comparison of winners and losers under the ten point must system,” *PLoS One*, vol. 12, no. 12, p. e0188675, 2017.
- [19] E. C. Dunn, “The manifestations of fatigue in amateur boxing performance,” 2019. [Online]. Available: Retrieved from <https://ro.ecu.edu.au/theses/2195>
- [20] L. Lu, F. M. Megahed, and L. A. Cavuoto, “Interventions to mitigate fatigue induced by physical work: A systematic review of research quality and levels of evidence for intervention efficacy,” *Human Factors: The Journal of the Human Factors and Ergonomics Society*, vol. 63, no. 1, pp. 151–191, 2021.
- [21] A. Sharotry, J. A. Jimenez, F. A. M. Mediavilla, D. Wierschem, R. M. Koldenhoven, and D. Valles, “Manufacturing operator ergonomics: A conceptual digital twin approach to detect biomechanical fatigue,” *IEEE Access*, vol. 10, pp. 12 774–12 791, 2022.
- [22] J. Z. Liu, R. W. Brown, and G. H. Yue, “A dynamical model of muscle activation, fatigue, and recovery,” *Biophysical journal*, vol. 82, no. 5, pp. 2344–2359, 2002.
- [23] T. Xia and L. A. Frey Law, “A theoretical approach for modeling peripheral muscle fatigue and recovery,” *Journal of Biomechanics*, vol. 41, no. 14, pp. 3046–3052, 2008.
- [24] L. A. Frey Law, J. M. Looft, and J. Heitsman, “A three-compartment muscle fatigue model accurately predicts joint-specific maximum endurance times for sustained isometric tasks,” *Journal of Biomechanics*, vol. 45, no. 10, pp. 1803–8, 2012.
- [25] I. Loi, E. I. Zacharaki, and K. Moustakas, “Machine learning approaches for 3d motion synthesis and musculoskeletal dynamics estimation: A survey,” *IEEE transactions on visualization and computer graphics*, vol. 30, no. 8, 08 2023.
- [26] A. Aristidou, A. Yiannakides, K. Aberman, D. Cohen-Or, A. Shamir, and Y. Chrysanthou, “Rhythm is a dancer: Music-driven motion synthesis with global structure,” *IEEE Transactions on Visualization and Computer Graphics*, pp. 1–1, 2021.
- [27] S. Starke, H. Zhang, T. Komura, and J. Saito, “Neural state machine for character-scene interactions,” *ACM Transactions on Graphics*, vol. 38, no. 6, p. 14, 2019.
- [28] S. Starke, Y. Zhao, T. Komura, and K. Zaman, “Local motion phases for learning multi-contact character movements,” *ACM Transactions on Graphics*, vol. 39, no. 4, p. 14, 2020.

- [29] S. Starke, Y. Zhao, F. Zinno, and T. Komura, "Neural animation layering for synthesizing martial arts movements," *ACM Transactions on Graphics*, vol. 40, no. 4, p. 16, 2021.
- [30] D. Zhou, X. Feng, P. Yi, X. Yang, Q. Zhang, X. Wei, and D. Yang, "3d human motion synthesis based on convolutional neural network," *IEEE Access*, vol. 7, pp. 66 325–66 335, 2019.
- [31] Q. Men, H. Shum, E. Ho, and H. Leung, "Gan-based reactive motion synthesis with class-aware discriminators for human-human interaction," 2021.
- [32] L. Mourot, L. Hoyet, F. L. Clerc, and P. Hellier, "Underpressure: Deep learning for foot contact detection, ground reaction force estimation and footskate cleanup," 2022. [Online]. Available: <https://arxiv.org/abs/2208.04598>
- [33] Y. Cai, Y. Wang, Y. Zhu, T.-J. Cham, J. Cai, J. Yuan, J. Liu, C. Zheng, S. Yan, H. Ding, X. Shen, D. Liu, and N. Thalmann, "A unified 3d human motion synthesis model via conditional variational auto-encoder," in *2021 IEEE/CVF International Conference on Computer Vision (ICCV)*, 2021, pp. 11 625–11 635.
- [34] Z. Zhou, Y. Wan, and B. Wang, "A unified framework for multimodal, multi-part human motion synthesis," 2023. [Online]. Available: <https://arxiv.org/abs/2311.16471>
- [35] S. Hou, H. Tao, H. Bao, and W. Xu, "A two-part transformer network for controllable motion synthesis," *IEEE Transactions on Visualization and Computer Graphics*, vol. 30, no. 8, pp. 5047–5062, 2024.
- [36] Z. Chai and H. Qin, "Dynamic motion transition: A hybrid data-driven and model-driven method for human pose transitions," *IEEE Transactions on Visualization and Computer Graphics*, pp. 1–14, 2024.
- [37] S. Raab, I. Leibovitch, G. Tevet, M. Arar, A. H. Bermanto, and D. Cohen-Or, "Single motion diffusion," 2023. [Online]. Available: <https://arxiv.org/abs/2302.05905>
- [38] S. Alexanderson, R. Nagy, J. Beskow, and G. E. Henter, "Listen, denoise, action! audio-driven motion synthesis with diffusion models," *ACM Trans. Graph.*, vol. 42, no. 4, 2023.
- [39] R. Dabral, M. H. Mughal, V. Golyanik, and C. Theobalt, "Mofusion: A framework for denoising-diffusion-based motion synthesis," in *Proceedings of the IEEE/CVF Conference on Computer Vision and Pattern Recognition (CVPR)*, June 2023, pp. 9760–9770.
- [40] X. Gao, Y. Yang, Z. Xie, S. Du, Z. Sun, and Y. Wu, "Guess: Gradually enriching synthesis for text-driven human motion generation," *IEEE Transactions on Visualization and Computer Graphics*, vol. 30, no. 12, pp. 7518–7530, 2024.
- [41] S. Lee, S. Lee, Y. Lee, and J. Lee, "Learning a family of motor skills from a single motion clip," *ACM Transactions on Graphics*, vol. 40, no. 4, pp. 1–13, 2021.
- [42] Z. Luo, J. Cao, J. Merel, A. Winkler, J. Huang, K. Kitani, and W. Xu, "Universal humanoid motion representations for physics-based control," 2024. [Online]. Available: <https://arxiv.org/abs/2310.04582>
- [43] X. Zhang, B. L. Bhatnagar, S. Starke, I. Petrov, V. Guzov, H. Dharmo, E. Pérez-Pellitero, and G. Pons-Moll, "Force: Dataset and method for intuitive physics guided human-object interaction," 2024. [Online]. Available: <https://arxiv.org/abs/2403.11237>
- [44] N. Cheema, R. Xu, N. H. Kim, P. Hämäläinen, V. Golyanik, M. Habermann, C. Theobalt, and P. Slusallek, "Discovering fatigued movements for virtual character animation," in *SIGGRAPH Asia 2023 Conference Papers*. New York, NY, USA: Association for Computing Machinery, 2023.
- [45] A. Seth, J. Hicks, T. Uchida, A. Habib, C. Dembia, J. Dunne, C. Ong, M. DeMers, A. Rajagopal, M. Millard, S. Hamner, E. Arnold, J. Yong, S. Lakshmikanth, M. Sherman, and S. Delp, "Opensim: Simulating musculoskeletal dynamics and neuromuscular control to study human and animal movement," *PLoS Computational Biology*, vol. 14, no. 7, p. e1006223, 2018.
- [46] M. Raissi, P. Perdikaris, and G. E. Karniadakis, "Physics informed deep learning (part I): data-driven solutions of nonlinear partial differential equations," *CoRR*, vol. abs/1711.10561, 2017. [Online]. Available: <http://arxiv.org/abs/1711.10561>
- [47] M. Raissi, P. Perdikaris, and G. E. Karniadakis, "Physics-informed neural networks: A deep learning framework for solving forward and inverse problems involving nonlinear partial differential equations," *Journal of Computational Physics*, vol. 378, pp. 686–707, 2019.
- [48] M. Mahmoudabadbozchelou, G. E. Karniadakis, and S. Jamali, "n-pinn: Non-newtonian physics-informed neural networks for complex fluid modeling," *Soft Matter*, vol. 18, no. 1, pp. 172–185, 2022.
- [49] H. Eivazi, Y. Wang, and R. Vinuesa, "Physics-informed deep-learning applications to experimental fluid mechanics," *Measurement science and technology*, vol. 35, no. 7, p. 075303, 2024.
- [50] A. Sedykh, M. Podapaka, A. Sagingalieva, K. Pinto, M. Pflitsch, and A. Melnikov, "Hybrid quantum physics-informed neural networks for simulating computational fluid dynamics in complex shapes," *Machine Learning: Science and Technology*, vol. 5, no. 2, p. 025045, May 2024. [Online]. Available: <http://dx.doi.org/10.1088/2632-2153/ad43b2>
- [51] C. Trahan, M. Loveland, and S. Dent, "Quantum physics-informed neural networks," *Entropy*, vol. 26, no. 8, p. 649, 2024.
- [52] K. Taneja, X. He, Q. He, and J.-S. Chen, "A multi-resolution physics-informed recurrent neural network: formulation and application to musculoskeletal systems," *Computational Mechanics*, vol. 73, no. 5, pp. 1125–1145, 2024.
- [53] R. Kumar, S. P. Muthukrishnan, L. Kumar, and S. Roy, "Predicting multi-joint kinematics of the upper limb from emg signals across varied loads with a physics-informed neural network," 2023. [Online]. Available: <https://arxiv.org/abs/2312.09418>
- [54] J. Zhang, Y. Zhao, T. Bao, Z. Li, K. Qian, A. Frangi, S. Xie, and E. Zhang, "Boosting personalized musculoskeletal modeling with physics-informed knowledge transfer," *IEEE Transactions on Instrumentation and Measurement*, vol. PP, pp. 1–1, 11 2022.
- [55] R. Kumar, A. Gupta, S. P. Muthukrishnan, L. Kumar, and S. Roy, "semg-driven physics-informed gated recurrent networks for modeling upper limb multi-joint movement dynamics," 2024. [Online]. Available: <https://arxiv.org/abs/2408.16599>
- [56] J. Zhang, Z. Ruan, Q. Li, and Z.-Q. Zhang, "Toward robust and efficient musculoskeletal modeling using distributed physics-informed deep learning," *IEEE Transactions on Instrumentation and Measurement*, vol. 72, pp. 1–11, 2023.
- [57] K. Cho, B. van Merriënboer, C. Gulcehre, D. Bahdanau, F. Bougares, H. Schwenk, and Y. Bengio, "Learning phrase representations using rnn encoder-decoder for statistical machine translation," in *Proceedings of the 2014 Conference on Empirical Methods in Natural Language Processing (EMNLP)*, 2014, pp. 1724–1734.
- [58] F. Chollet, *Deep Learning with Python*. New York: Manning Publications, 2017.
- [59] M. Kapadia, A. Shoulson, F. Durupinar, and N. I. Badler, "Authoring multi-actor behaviors in crowds with diverse personalities," *Modeling, Simulation and Visual Analysis of Crowds: A Multidisciplinary Perspective*, pp. 147–180, 2013.
- [60] A. Rajagopal, C. L. Dembia, M. S. DeMers, D. D. Delp, J. L. Hicks, and S. L. Delp, "Full-body musculoskeletal model for muscle-driven simulation of human gait," *IEEE transactions on biomedical engineering*, vol. 63, no. 10, pp. 2068–2079, 2016.
- [61] N. Cheema, L. A. Frey-Law, K. Naderi, J. Lehtinen, P. Slusallek, and P. Hämäläinen, "Predicting mid-air interaction movements and fatigue using deep reinforcement learning," in *Proceedings of the 2020 CHI Conference on Human Factors in Computing Systems*, 2020, pp. 1–13.
- [62] L. A. Frey-Law, M. Schaffer, and F. K. Urban III, "Muscle fatigue modelling: Solving for fatigue and recovery parameter values using fewer maximum effort assessments," *International journal of industrial ergonomics*, vol. 82, p. 103104, 2021.
- [63] M. Burnley, "Estimation of critical torque using intermittent isometric maximal voluntary contractions of the quadriceps in humans," *Journal of Applied Physiology*, vol. 106, no. 3, pp. 975–983, 2009.
- [64] F. Chollet *et al.* (2015) Keras. [Online]. Available: <https://github.com/fchollet/keras>
- [65] D. P. Kingma and J. Ba, "Adam: A method for stochastic optimization," 2014. [Online]. Available: <https://arxiv.org/abs/1412.6980>
- [66] M. Schuster and K. Paliwal, "Bidirectional recurrent neural networks," *IEEE Transactions on Signal Processing*, vol. 45, no. 11, pp. 2673 – 2681, 1997.
- [67] I. Ihianle, A. Nwajana, S. Ebebuwa, R. Otuka, K. Owa, and M. Orisatoki, "A Deep Learning Approach for Human Activities Recognition From Multimodal Sensing Devices," *IEEE Access*, vol. 8, pp. 179 028–179 038, 2020.
- [68] Z. Cui, R. Ke, Z. Pu, and Y. Wang, "Deep bidirectional and unidirectional lstm recurrent neural network for network-wide traffic speed prediction," 2018. [Online]. Available: <https://arxiv.org/abs/1801.02143>
- [69] J. K. Haas, "A history of the unity game engine," 2014.
- [70] J. R. Fuller, K. V. Lomond, J. Fung, and J. N. Côté, "Posture-movement changes following repetitive motion-induced shoulder muscle fatigue," *Journal of Electromyography and Kinesiology*, vol. 19, no. 6, pp. 1043–1052, 2009.
- [71] W. J. Grantham, I. R. Byram, M. C. Meadows, and C. S. Ahmad, "The impact of fatigue on the kinematics of collegiate baseball pitchers," *Orthopaedic journal of sports medicine*, vol. 2, no. 6, p. 2325967114537032, 2014.

- [72] Z. Wang, J. Chai, and S. Xia, "Combining recurrent neural networks and adversarial training for human motion synthesis and control," *IEEE Transactions on Visualization and Computer Graphics*, vol. 27, no. 1, pp. 14–28, 2019.